SENSITIVITY ANALYSIS FOR STEREOTOMOGRAPHY IN ELLIPTIC AND ANELLIPTIC MEDIA

B. S. S. Barbosa, J. C. Costa, E. N. S. Gomes, and J. Schleicher

email: *jesse@ufpa.br*

keywords: *Stereotomography, Anisotropy, Sensitivity Analysis*

ABSTRACT

Stereotomography is extended to general anisotropic models and implemented for elliptical and anelliptical anisotropy. Elliptical and anelliptical models depend on three parameters only, which makes them less sensitive to ambiguity due to limited coverage of surface seismic experiments than transversely isotropic or orthorhombic models. The corresponding approximations of the slowness surface restrict the validity of the present approach to qP events and mild anisotropy. Numerical experiments show the potential and the limitations of stereotomography for estimating macrovelocity models in the presence of anisotropy as well as the importance of transmission events from multiple-offset VSP experiments for the success of the approach.

INTRODUCTION

The determination of a macrovelocity model is essential for time and depth imaging of seismic reflectors in the earth. Among the many methods that try to to achieve this aim are so-called tomographic methods that are based on the inversion of traveltimes of seismic reflection events. One of these is stereotomography, which uses slowness vector components to improve and stabilize the traveltime inversion. Stereotomography was initially proposed by Billette and Lambaré (1998) as a robust tomographic method for estimating velocity macro models from seismic reflection data. They had recognized the potential efficiency of traveltime tomography (Bishop et al., 1985; Farra and Madariaga, 1988) but also the difficulties associated with a highly interpretative picking. The selected events have to be tracked over a large extent of the pre-stack data cube, which is quite difficult for noisy or complex data. The idea is to use locally coherent events characterized by their slopes in the pre-stack data-volume. Such events can be interpreted as pairs of ray segments and provide independent information about the velocity model.

Recently, Billette et al. (2003) demonstrated the successful use of stereotomography to recover isotropic background media. According to Gosselet et al. (2005), the use of reflection events only is insufficient to recover anisotropic models. Here, we study the limitations of stereotomography applied in anisotropic media, using reflected *and* transmitted events. For this purpose, we use approximations for weak elliptic and anelliptic anisotropy that are valid for qP waves.

Any tomographic method is based on ray theory. Our approach follows the lines of Farra and Madariaga (1987) who applied perturbation theory to the Hamiltonian systems that describe the rays in media with arbitrary anisotropy (Goldstein, 1980). Perturbation theory allows to calculate linear approximations to the observed data, the so-called Fréchet derivatives. Here, we extend the work of Farra and Madariaga (1987) to arbitrary anisotropy and restrict it later on for application purposes to elliptic and anelliptic media.

STEREOTOMOGRAPHY IN ANISOTROPIC MEDIA

Stereotomography differs from conventional reflection tomography by the data that are used for the inversion (Billette et al., 2003). Firstly, the traveltimes are picked from locally coherent events that are

interpreted as primary reflections or diffractions. Secondly, in-line slowness vectors components of these events, detected in common-shot or common-receiver gathers, are used in addition to positions and traveltimes of sources and receivers. Thus, the data space is given by

$$\mathbf{d} = \left[(\mathbf{x}^s, \mathbf{x}^r, s^s, s^r, T^{sr})_n\right] \qquad (n = 1, \ldots, N) \; . \tag{1}$$

where $\mathbf{x}^s$ and $\mathbf{x}^r$ are the source and receiver positions, T^{sr} are the traveltimes, and s^s and s^r are the slowness-vector projections into the receiver line. Moreover, N is the number of selected events.

Stereotomography also uses a different model parameterization than conventional reflection tomography. In 2D, the model to be estimated includes: the parameters describing the velocity model, $\mathbf{p}$, the scattering-point coordinates, $\mathbf{X}$, the emergence angles, θ^s and θ^r, and the ray traveltimes, τ^s e τ^r. In other words, the model vector is

$$\mathbf{m} = \{\mathbf{p}, (\mathbf{X}, \theta^s, \theta^r, \tau^s, \tau^r)_n\} \qquad (n = 1, \ldots, N) \; . \tag{2}$$

To solve the inverse problem using linear iterations, an initial reference model must be given. In this model $\mathbf{m}_0$, ray tracing is performed to calculate the synthetic data, equation (1), denoted as $\mathbf{d}^c$. The difference between the observed and calculated data, $\mathbf{d}^o - \mathbf{d}^c$, defines the deviation $\delta\mathbf{d}$.

This deviation is modeled in linear approximation as

$$\delta\mathbf{d} = \mathcal{D}\mathbf{F}(\mathbf{m}_0)\delta\mathbf{m} \; , \tag{3}$$

where $\mathcal{D}\mathbf{F}$ denotes the approximate operator describing the direct problem under variation of the reference model $\mathbf{m}_0$. The operator $\mathcal{D}\mathbf{F}(\mathbf{m}_0)$ is known as the Fréchet derivative (see, e.g., Menke, 1989). The solution of the linear system in equation (3) determines a new reference model

$$\mathbf{m}_0^{new} = \mathbf{m}_0 + \delta\mathbf{m}. \tag{4}$$

The process continues iteratively until the norm of the deviation $\|\delta\mathbf{d}\|$ is smaller than a given tolerance value (in case of convergence) or until a maximum number of steps. In this work, we use the standard L_2 norm (Menke, 1989).

Rays in anisotropic media

The ray tracing system in generally anisotropic media can be represented as (Červený, 2001)

$$\frac{d\mathbf{x}}{d\tau} = \nabla_{\mathbf{s}}\mathcal{H} \; , \qquad \frac{d\mathbf{s}}{d\tau} = -\nabla_{\mathbf{x}}\mathcal{H} \; , \tag{5}$$

where $\nabla_{\mathbf{x}}$ and $\nabla_{\mathbf{s}}$ represent the gradients with respect to the position and slowness vectors, $\mathbf{x}$ and $\mathbf{s}$, respectively, and where τ is the traveltime along the ray. Moreover, $\mathcal{H}(\mathbf{x}, \mathbf{s}; \mathbf{p}) = 0$ along the ray. In tomographic applications, this system (5) is solved numerically.

Upon perturbation of the medium parameters $\mathbf{p}$, the position and slowness vectors of a ray get perturbed. Retaining only first-order effects in these perturbations $\delta\mathbf{p}$, $\delta\mathbf{x}$ and $\delta\mathbf{s}$, the system becomes

$$\frac{d}{d\tau}\begin{bmatrix} \delta\mathbf{x} \\ \\ \delta\mathbf{s} \end{bmatrix} = \begin{bmatrix} \nabla_{\mathbf{s}}\nabla_{\mathbf{x}}^T\mathcal{H} & \nabla_{\mathbf{s}}\nabla_{\mathbf{s}}^T\mathcal{H} \\ \\ -\nabla_{\mathbf{x}}\nabla_{\mathbf{x}}^T\mathcal{H} & -\nabla_{\mathbf{x}}\nabla_{\mathbf{s}}^T\mathcal{H} \end{bmatrix}\begin{bmatrix} \delta\mathbf{x} \\ \\ \delta\mathbf{s} \end{bmatrix} + \begin{bmatrix} \nabla_{\mathbf{s}}\nabla_{\mathbf{p}}^T\mathcal{H}\delta\mathbf{p} \\ \\ -\nabla_{\mathbf{x}}(\nabla_{\mathbf{p}}^T\mathcal{H}\delta\mathbf{p}) \end{bmatrix} . \tag{6}$$

Initial conditions

Initial conditions for $\delta\mathbf{x}$ e $\delta\mathbf{s}$ can be established upon requiring that the first-order perturbations of the Hamiltonian at the starting point must be zero. This condition guarantees that the paraxial rays satisfy, to the first order, the Hamiltonian equations. For stereotomography, it is necessary to integrate the above

system (6) for one initial condition for each possible perturbations. Therefore, the determination can be reduced to three cases:
(1) Perturbation of the slowness direction:

$$\delta\mathbf{s} = s\left(\mathbf{I} - \frac{\mathbf{n}\,\nabla_{\mathbf{s}}^T\mathcal{H}}{\nabla_{\mathbf{s}}^T\mathcal{H}\,\mathbf{n}}\right)\frac{d\mathbf{n}}{d\theta}\delta\theta\ . \tag{7}$$

(2) Perturbation of the diffraction point position:

$$\delta\mathbf{s} = -\frac{\nabla_{\mathbf{s}}\mathcal{H}}{\|\nabla_{\mathbf{s}}\mathcal{H}\|}\ \frac{\nabla_{\mathbf{x}}^T\mathcal{H}\delta\mathbf{X}}{\|\nabla_{\mathbf{s}}\mathcal{H}\|}\ , \tag{8}$$

(3) Perturbation of the elastic parameters:

$$\delta\mathbf{s} = -\frac{\nabla_{\mathbf{s}}\mathcal{H}}{\|\nabla_{\mathbf{s}}\mathcal{H}\|}\ \nabla_{\mathbf{p}}^T\mathcal{H}\delta\mathbf{p}/\|\nabla_{\mathbf{s}}\mathcal{H}\|. \tag{9}$$

With these initial conditions, the system in equation (6) can be integrated along a ray in the reference medium. In this way, the Fréchet derivatives with respect to the perturbations of the initial position, initial angle, and elastic parameters can be numerically evaluated. System (6) can be efficiently solved for each choice of initial conditions by means of the propagator method (Červený, 2001). With the central ray, i.e., $\mathbf{x}(\tau)$ and $\mathbf{s}(\tau)$, supposed to be known, system (6) takes the form

$$\frac{d\mathbf{y}}{d\tau} = \mathbf{A}(\tau)\mathbf{y} + \mathbf{f}(\tau)\ , \tag{10}$$

where

$$\mathbf{A}(\tau) = \begin{bmatrix} \nabla_{\mathbf{s}}\nabla_{\mathbf{x}}^T\mathcal{H} & \nabla_{\mathbf{s}}\nabla_{\mathbf{s}}^T\mathcal{H} \\ -\nabla_{\mathbf{x}}\nabla_{\mathbf{x}}^T\mathcal{H} & -\nabla_{\mathbf{x}}\nabla_{\mathbf{s}}^T\mathcal{H} \end{bmatrix}\ , \qquad \mathbf{y} = \begin{bmatrix} \delta\mathbf{x} \\ \delta\mathbf{s} \end{bmatrix}\ , \qquad \text{and} \qquad \mathbf{f} = \begin{bmatrix} \nabla_{\mathbf{s}}(\nabla_{\mathbf{p}}^T\mathcal{H}\delta\mathbf{p}) \\ -\nabla_{\mathbf{x}}(\nabla_{\mathbf{p}}^T\mathcal{H}\delta\mathbf{p}) \end{bmatrix}\ . \tag{11}$$

Equation (10) is a system of linear ordinary differential equations. The propagator methods allow to represent the solution to this system in an interval (τ_0, τ), satisfying the initial condition $\mathbf{y}(\tau_0) = \mathbf{y}_0$, as

$$\mathbf{y}(\tau) = \mathbf{P}(\tau, \tau_0)\mathbf{y}_0 + \int_{\tau_0}^{\tau} \mathbf{P}(\tau, \xi)\mathbf{f}(\xi)d\xi\ . \tag{12}$$

The initial condition for the propagator matrix $\mathbf{P}(\tau, \tau_0)$ is then $\mathbf{P}(\tau_0, \tau_0) = \mathbf{I}$, where $\mathbf{I}$ is the identity matrix. Numerically, $\mathbf{P}(\tau, \tau_0)$ can be determined using Runge-Kutta schemes. For stereotomography, this approach has the advantage that the propagator matrix $\mathbf{P}(\tau, \tau_0)$ can be determined independently of $\mathbf{y}_0$, which means that it needs to be calculated only once.

The integration of system (6) is based on the assumption that the elastic parameters vary smoothly. Actually, they need to be second-order differentiable. Moreover, the model needs to be specified by a finite number of parameters. To satisfy these conditions, the parameters must be interpolated. In our implementation, each medium parameter is represented using the tensor product of third-order B-splines as

$$p_m(x_1, x_3) \quad = \quad \sum_{\alpha=1}^{N_1}\sum_{\beta=1}^{N_2} p_m^{\alpha\beta}B_\alpha(x_1)B_\beta(x_3)\ , \tag{13}$$

where the functions $B_\gamma(x_j)$ are the base functions of the interpolator along x_j and N_j indicates the number of base functions in that direction. Moreover, the $p_m^{\alpha\beta}$ are the interpolation coefficients that constitute the medium parameters to be estimated by stereotomography.

Hamiltonians

A possible form for the Hamiltonian in anisotropic elastic media is

$$\mathcal{H}(\mathbf{x},\mathbf{s}) = |a_{ijkl}(\mathbf{x})s_j s_l - \delta_{ik}| = 0\,, \tag{14}$$

where $a_{ijkl}(\mathbf{x})$ are the density-normalized components of the stiffness tensor (Musgrave, 1970). To reduce the number of parameters to invert for, we study only the inversion of qP events in the elliptical approximation (Dellinger et al., 1993)

$$\mathcal{H}(\mathbf{x},\mathbf{s}) = \frac{1}{2}[p_1(\mathbf{x})s_1^2 + p_2(\mathbf{x})s_3^2 + 2\,p_3(\mathbf{x})s_1\,s_3 - 1] = 0\,, \tag{15}$$

and the anelliptical approximation for vertically transversely isotropic (VTI) media (Schoenberg and deHoop, 2000)

$$\mathcal{H}(\mathbf{x},\mathbf{s}) = \frac{1}{2}[p_1(\mathbf{x})s_1^2 + p_2(\mathbf{x})s_3^2 - (p_1(\mathbf{x})p_2(\mathbf{x}) - p_3^2(\mathbf{x}))\,s_1^2 s_3^2 - 1] = 0\,. \tag{16}$$

The elliptic approximation can represent slowness surface segments with arbitrary orientation. The anelliptic approximation is very good for qP waves in VTI media with mild anisotropy (Schoenberg and deHoop, 2000). This class includes many shales, which are the sedimentary rocks that exhibit the greatest degree of anisotropy.

Here, the medium parameters p_1 and p_2 are the squares of the horizontal and vertical phase velocities, respectively. In an elliptic medium, i.e., in equation (15), parameter p_3 indicates the orientation of the ellipse. In the anelliptical medium, i.e., in equation (16), p_3 is determined by the phase velocity at 45^o.

Resolution analysis

The Fréchet derivatives contain all information about the incompleteness of the data for the estimation of $\delta\mathbf{m}$. Generally, the linear system in equation (3) is ill-conditioned because of the limited ray coverage in the model (Nolet, 1987). The resolution matrix $\mathbf{R} = \mathbf{V}_r\mathbf{V}_r^T$ can be determined from the singular-value decomposition of $\mathcal{D}\mathbf{F}$ (Lawson and Hanson, 1974; Menke, 1989). Here, $\mathbf{V}_r$ is a submatrix of the orthogonal matrix $\mathbf{V}$ of dimension N_m, the columns of which are the eigenvectors of the space $\mathcal{D}^T\mathbf{F}\mathcal{D}\mathbf{F}$. $\mathbf{V}_r$ is associated with the singular values greater than a value λ_{rr}, which is chosen by the prescription of an acceptable condition number for $\mathcal{D}\mathbf{F}$.

The lines of the resolution matrix $\mathbf{R}$ indicate which model parameters are well resolved. The closer $\mathbf{R}$ is to the identity matrix, the better the parameter resolution and, thus, the quality of the inversion result. Nonzero off-diagonal elements represent linear dependence of the corresponding parameters that therefore cannot be well resolved.

Resolution analysis of the Fréchet derivatives using singular value decomposition (SVD) is useful to determine the limits of stereotomography for anisotropic model reconstruction. We use a homogeneous isotropic medium as a reference model and computed the Fŕechet derivatives for an elliptic and an anelliptic media. Two acquisition geometries were considered. First, a CMP array and a single diffraction event, the scatter is located at 1.5 km in depth, offsets vary form 1 km to 7 km, equally spaced at every 1 km. Second, we add to the previous data transmission data from a VSP acquisition, the well is located along the midpoint of the split-spread array, the source is at the surface 1 km from the well head and the two receivers are located along the well at 500 m and 2 km. The vertical slowness component is taken for each transmission data.

We compute the resolution matrix for each set of acquisition geometry for the elliptic and anelliptic models. For the SVD analysis, the stereotomography model parameters in vector $\mathbf{m}$ are ordered as: $m_1 \equiv p_1$, $m_2 \equiv p_2$, $m_3 \equiv p_3$, and $m_{6i-2} \equiv X_1^i$, $m_{6i-1} \equiv X_3^i$, $m_{6i} \equiv \theta_i^s$, $m_{6i+1} \equiv \theta_i^r$, $m_{6i+2} \equiv \tau_i^s$, $m_{6i+3} \equiv \tau_i^r$, with $i = 1,\ldots,N$. Therefore, the medium parameters are equal to m_1, m_2 and m_3. The remaining parameters for each picked event are diffractor position, slowness angles and traveltime for each ray branch. For transmission data we add to the model parameter vector $\mathbf{m}$ the transmission traveltime, τ_t, and the ray angle at the source, $theta_t$.

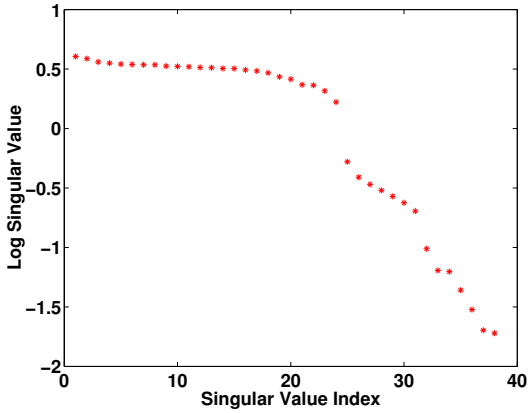

Figure 1: Non-zero singular values in non-increasing order for a single diffraction event in elliptical media. Sources and receivers are in a CMP array.

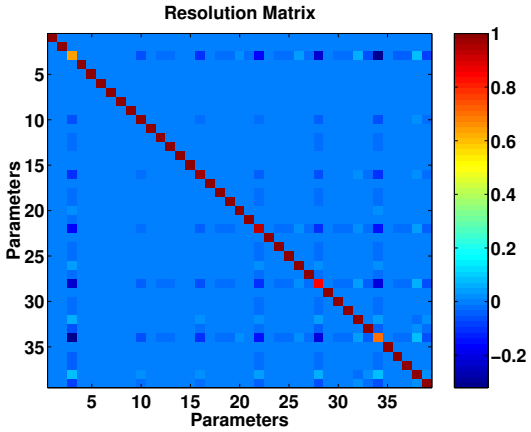

Figure 2: Resolution matrix computed dropping the zero singular value in Figure 1. Single diffraction event in a homogeneous elliptical medium.

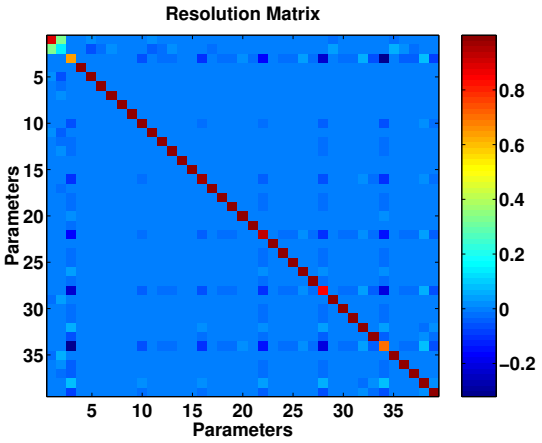

Figure 3: Resolution matrix computed dropping the two smaller singular value in Figure 1.

* **Elliptical medium**

Figure 1 shows the nonzero singular values for the single diffraction event and CMP acquisition geometry. The smallest singular value is zero. This indicates that the corresponding parameter cannot be recovered from data. Figure 2 shows the resolution matrix computed dropping the zero singular value. From the rows of resolution matrix, we see that the most poorly resolved parameter is p_3, which controls the tilt of the ellipse. This parameter is coupled with the position of the diffraction points, the slowness phase angles θ_s and θ_r, and the traveltimes on each ray branch connecting the diffractors to sources and receivers, τ_s and τ_r. Figure 3 shows the resolution matrix computed dropping the two smallest singular values. This time, besides the orientation of the ellipse, the vertical slowness, p_2, is poorly resolved. These results indicate that the ellipse orientation is the parameter that is most difficult to recover from the data, followed by the vertical phase velocity.

Figure 4 shows the singular values after adding the transmission data to the single diffraction event and CMP acquisition geometry. This time there is no zero singular value, and the conditioning of the matrix is greatly improved. The condition number of the matrix is 430. Figure 5 shows the resolution matrix computed dropping the smallest singular value. Again the parameters p_2 and p_3, i.e., the vertical phase velocity and the orientation of the ellipse, are strongly coupled. However, their coupling to the diffractor position is much reduced. The introduction of transmission data improves the conditioning and reduces the linear dependence among parameters.

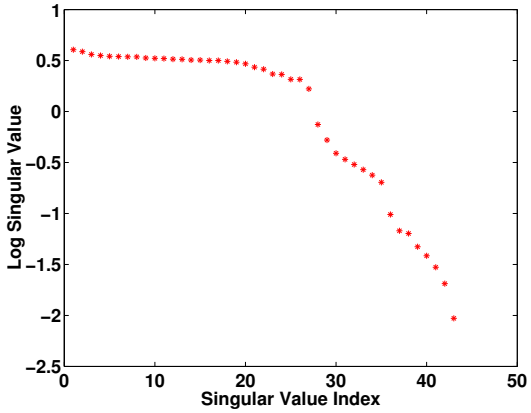

Figure 4: Singular values in non increasing order with transmission data for a VSP geometry is added to the previous surface data.

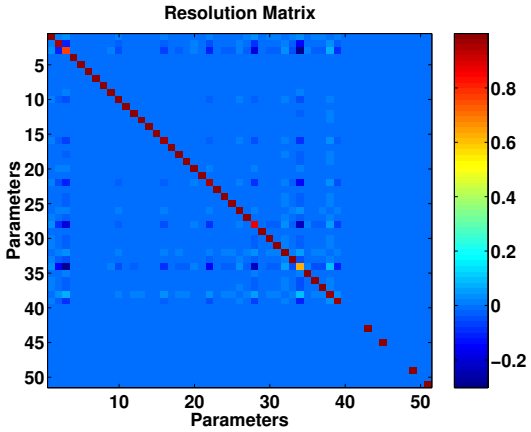

Figure 5: Resolution matrix computed dropping the smallest singular value in Figure 4.

* **Anelliptical medium**

Figure 6 shows the singular values for the single diffraction event and CMP acquisition geometry in an anelliptic medium. There is no zero singular value this time and the condition number is 430. Figure 7 shows the resolution matrix computed dropping the smallest singular value. The row of the resolution matrix the parameters with the poorest resolution corresponds to parameter p_2, the square of vertical phase velocity. It is most strongly coupled with parameter p_3, the phase velocity in the diagonal direction, and the depth of the diffractors. These results indicate that stereotomography can recover the medium parameters and diffractors position in an anelliptical medium. In the presence of noise, the vertical phase velocity is the most poorly resolved parameter, followed by the diagonal phase velocity and the diffractor depth.

Figure 8 shows the resolution matrix computed dropping the last two singular values. The condition number is now 210. Still, p_2 and p_3 are the parameters with the poorest resolution. These parameters are strongly coupled with the diffractor depth, X_3, and the medium parameter p_1. The horizontal coordinate of the reflector, X_1, the slowness phase angles, θ_s and θ_r, and the traveltimes on each ray branch connecting the diffractor to sources and receivers, τ_s and τ_r also loose resolution. Note that the resolution of the latter parameters decreases with increasing offset.

Figure 9 shows the singular values when we add the transmission data to the surface CMP data from the single diffraction event. The condition number improves and is equal to 285, as one can see comparing these singular values with those in Figure 6. Figure 10 shows the resolution matrix computed dropping the smallest singular value. The parameter p_3 is coupled with p_1 and the diffractors depth. As in the elliptic case, the addition of transmission data improves conditioning and reduces the linear dependence among parameters.

Summarizing, these initial experiments with single checkshots and single diffractors demonstrated that (a) estimation of anisotropic models using only reflection and diffraction events and surface acquisition geometry cannot recover stereotomography parameters in tilted elliptical media; (b) estimation of stereotomography parameters in anelliptical media using only reflection and diffraction events and surface acquisition geometry is possible but can be ill-conditioned; (c) the inclusion of transmission events from VSP experiments improves the conditioning of stereotomography; (d) the determination of the orientation of the slowness curve together with the position of the diffraction or reflection point is ill-conditioned.

Regularization

Due to the incompleteness of the data, additional conditions that take desirable properties of the solution into account, must be incorporated into the objective function. To reduce the ambiguity, three kinds of regularization are used, two of which minimize the medium heterogeneity and anisotropy, while the third one maximizes the diffractor focusing. Denoting the average diffractor position of diffractor number i by

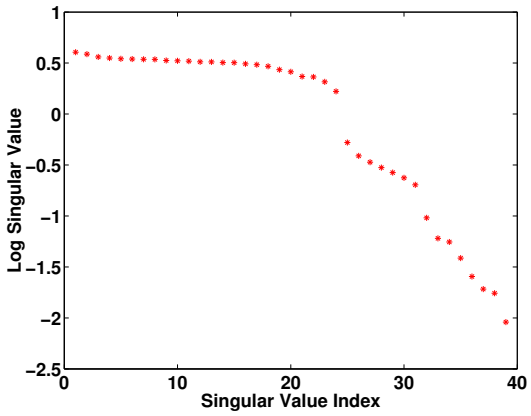

Figure 6: Singular values in non increasing order for a single diffraction event in an anelliptical medium.

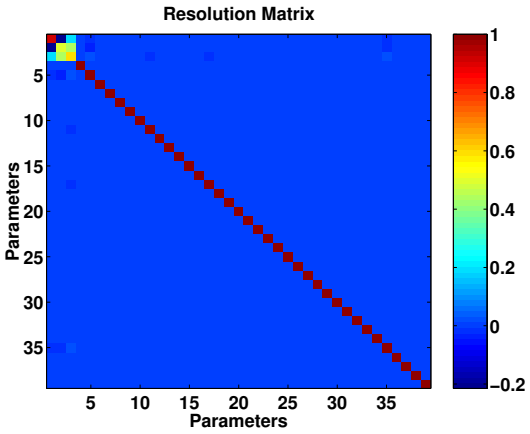

Figure 7: Resolution matrix computed dropping the smallest singular value in Figure 6.

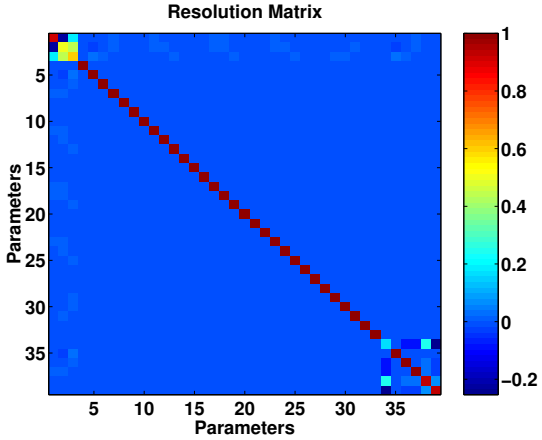

Figure 8: Resolution matrix computed dropping the two smaller singular value in Figure 6.

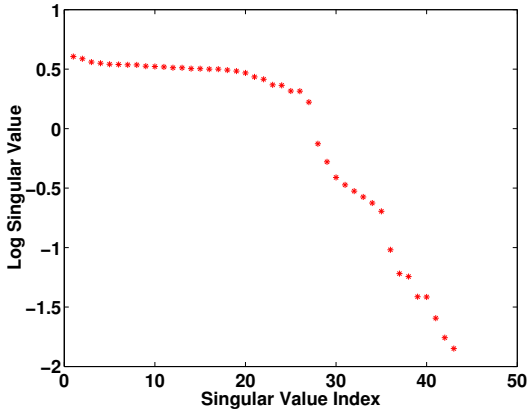

Figure 9: Singular values in non increasing order with transmission data for a VSP geometry is added to the previous surface data.

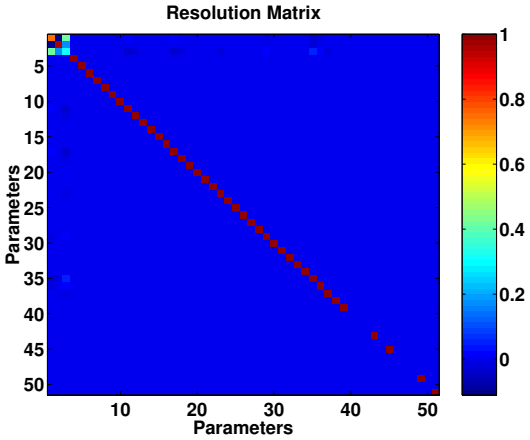

Figure 10: Resolution matrix computed dropping the smallest singular value in Figure 9.

$\langle \mathbf{X}^i \rangle$, the focusing is maximized if

$$\sum_{j=1}^{N_i} \|\mathbf{X}_j^i - \langle \mathbf{X}^i \rangle\|_2^2 \tag{17}$$

is minimized. Denoting the operators that minimize spatial derivatives by $\mathbf{D}_1^{(n)}$ and $\mathbf{D}_3^{(n)}$, and the one minimizing anisotropy by $\mathbf{D}_{iso}$, the regularized objective function for anisotropic stereotomography can be written as

$$\begin{aligned} \Phi(\mathbf{m};\lambda_i) \quad = \quad & \|\mathbf{d} - \mathbf{F}(\mathbf{m})\|_2^2 + \lambda_0^2 \|\mathbf{m} - \mathbf{m}_0\|_2^2 \\ & + \lambda_1^2 \|\mathbf{D}_1^{(n)} \mathbf{p}\|_2^2 + \lambda_2^2 \|\mathbf{D}_3^{(n)} \mathbf{p}\|_2^2 + \lambda_3^2 \|\mathbf{D}_{iso} \mathbf{p}\|_2^2 \\ & + \lambda_4^2 \sum_{i=1}^{N_{events}} \sum_{j=1}^{N_i} \|\mathbf{X}_j^i - \langle \mathbf{X}^i \rangle\|_2^2 \,, \end{aligned} \tag{18}$$

where the λ_i are Lagrangian multipliers that weight the contributions to the objective function.

SYNTHETIC DATA EXAMPLE

The described stereotomography algorithm was tested on a number of synthetic models, comparing the isotropic, elliptic, and anelliptic inversion. The data were modeled using the anisotropic ray-tracing code ANRAY of Gajewski and Pšenčík (1990).

In all tests, the VTI models were parametrized for inversion by 49 coefficients of the B-splines parametrization (13), specified on a regular 7×7 grid. The weights for the regularization terms in equation (18) were chosen as $\lambda_0 = 0.01$, $\lambda_1 = 0.01$, $\lambda_2 = 0.01$, and $\lambda_4 = 0.01$. In all cases, the inversion started from a homogeneous, isotropic initial model with velocity 3.0 km/s. In the following, typical results of stereotomographic inversion are presented for one of these models.

This model is a heterogeneous, weakly anisotropic VTI medium with Thomsen parameters (Thomsen, 1986) of $\epsilon = \delta = 0.189$ and $\gamma = 0.175$. The model has covers a subsurface region of 6 km x 3 km with diffraction points at the positions D_1 =(0.7 km, 2.9 km), D_2 =(1.2, 1.0), D_3 =(2.2 km, 1.7 km), D_4 = (3.8 km, 0.5 km), D_5 = (4.3 km, 1.5 km), D_6 = (4.8 km, 1.0 km), and D_7 =(5.3 km, 2.9 km). The surface data were simulated for a CMP situated at $x_m = 3.0$ km. The vertical and horizontal velocities in the model are depicted in Figures 11 and 12, respectively. Also shown in Figure 11 are the positions of the diffractors and the a subset of the rays used for tomography.

Figure 13 shows the result of isotropic stereotomography. The depicted ray families indicate the focusing behavior of the diffractors. We observe that the depth of the diffractors is systematically overestimated. This is an effect of the influence of the horizontal velocity which is larger than the vertical velocity in this model. The relative error, depicted in Figure 14, shows a large deviation from the vertical velocity, with maximum error in the order of 40%. When comparing the reconstructed isotropic model to the exact horizontal velocity model (see Figure 15), we see that above 1.0 km, the error is reduced. We may conclude that in the shallow part, isotropic stereotomography is more strongly influenced by horizontal than vertical velocities.

The vertical velocity model reconstructed with elliptic stereotomography is shown in Figure 16. The result presents very small lateral variations in the regions with high ray coverage. The depth of the diffractors is better estimated, although the focusing of the deeper ones, where few rays are available, is still poor. The quality of the velocities can be judged in Figure 17, which shows the relative error. We see that errors do not exceed 8% in regions with high ray coverage. The horizontal velocities from elliptic stereotomography are depicted in Figure 18. We recognize the recovery of the direction of the velocity gradient, but the failure to recover its strength. The errors, depicted in Figure 19 are smaller than 6% down to a depth of 1.5 km and become higher only in undersampled regions. From these results, we conclude that elliptic stereotomography does a better job in estimating the vertical than the horizontal velocity.

Although the model was chosen to be elliptically anisotropic, for completeness also an anelliptic stereotomography has been carried out. The resulting vertical velocity is depicted in Figure 20. We observe an even better depth estimation and focusing of the diffractors. As before, the result is worse in regions with lower ray coverage. However, the velocities are worse than the ones from elliptic stereotomography.

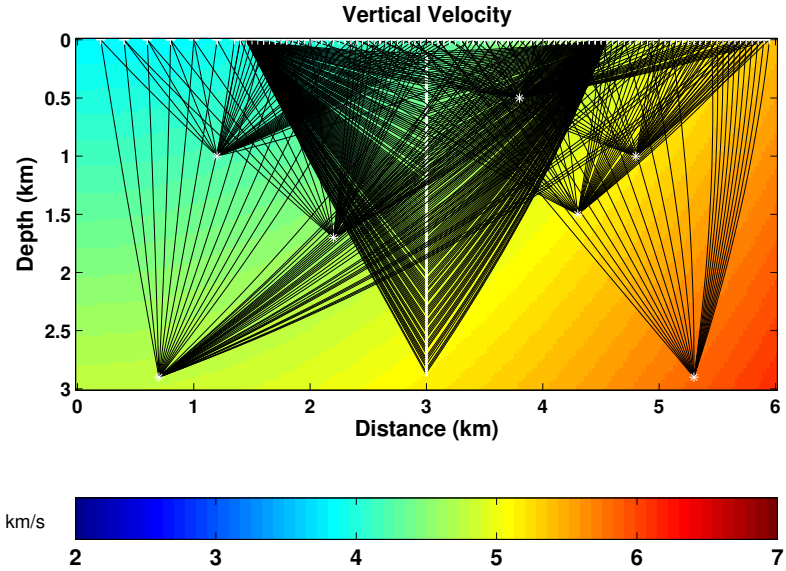

Figure 11: Model: Vertical velocity with a gradient towards the lower right corner. Also shown are the diffraction points (asterisks) and some ray families used for the tomographic inversion. The colorbar is the same for all subsequent velocity figures.

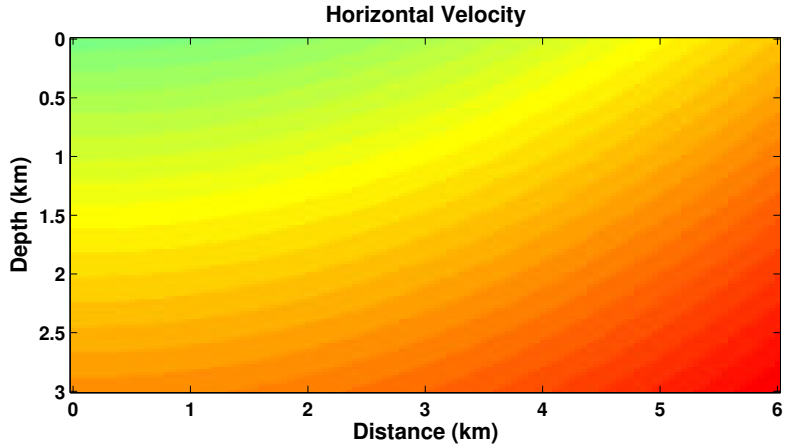

Figure 12: Model: Horizontal velocity.

The relative error is shown in Figure 21. We see that the variation of the model is strongly underestimated. Finally, Figure 22 and Figure 23 show the recovered horizontal velocity and the respective error. Although the horizontal velocity shows a similar variation to the original model in the region with highest ray coverage, the error is still higher than the one for elliptic stereotomography.

In summary, stereotomography works best where ray coverage is high. In such regions, anisotropic properties of the medium can be recovered to a certain degree. It is interesting to observe that in all our synthetic tests, even where the original model is anelliptic, elliptic stereotomography gave the smallest errors. A possible remedy for this might be the use of more transmission data in the inversion.

CONCLUSIONS

We have extended stereotomography to generally anisotropic media and implemented the corresponding inversion for two types of approximations for qP-wave slowness surfaces. The elliptic and anelliptic approximations represent the slowness surface as an ellipse of arbitrary orientation and a quartic surface with fixed orientation, respectively.

An analysis of the resolution matrix for experiments with single checkshots and single diffractors demonstrated that (a) estimation of anisotropic models using only reflection and diffraction events and

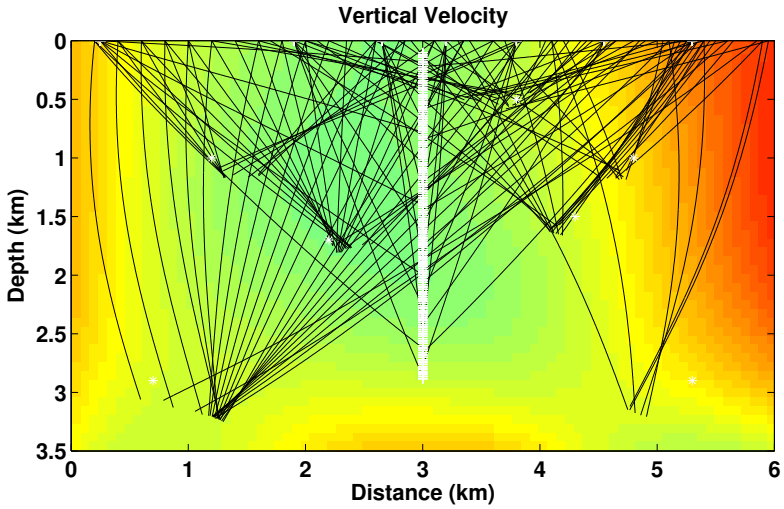

Figure 13: Velocity as result of isotropic stereotomography.

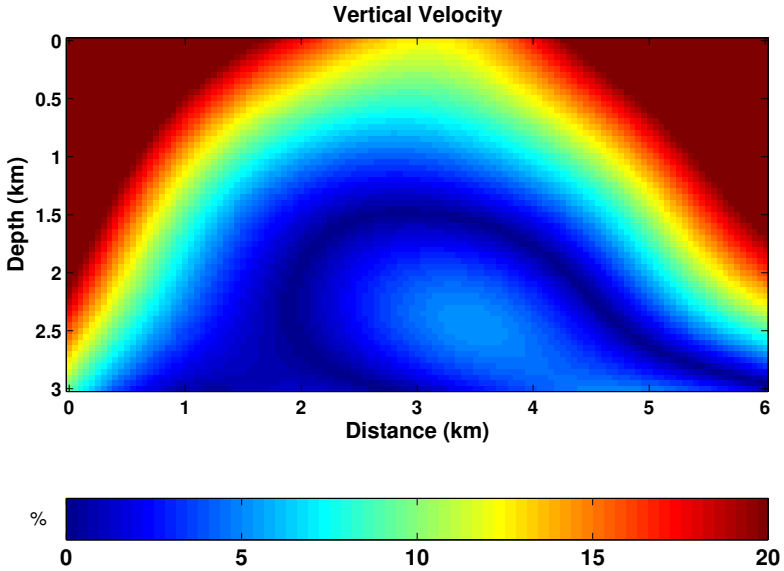

Figure 14: Relative error of vertical velocity from isotropic stereotomography. The colorbar is the same for all subsequent error figures.

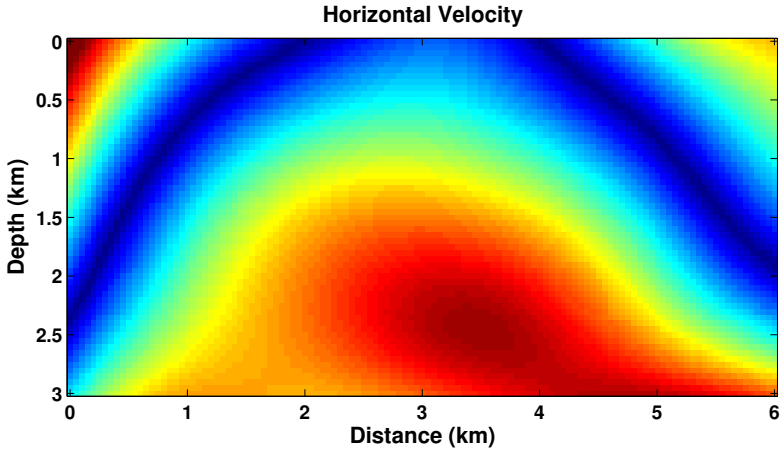

Figure 15: Relative error of horizontal velocity from isotropic stereotomography.

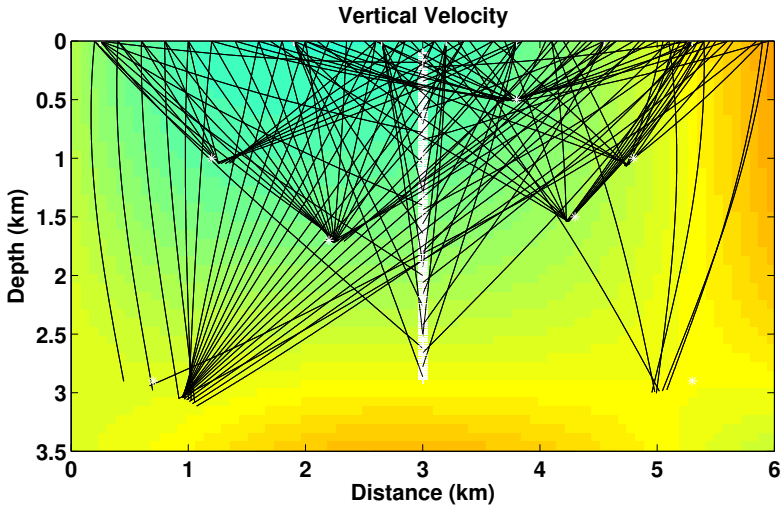

Figure 16: Vertical velocity as result of elliptic stereotomography.

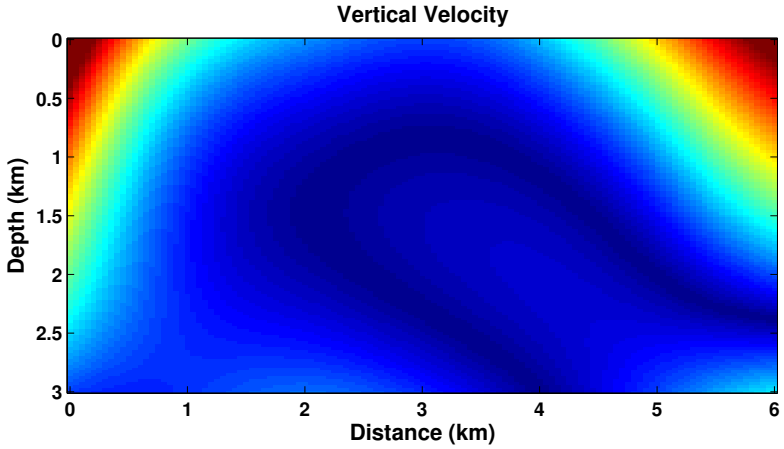

Figure 17: Relative error of vertical velocity from elliptic stereotomography.

surface acquisition geometry cannot recover stereotomography parameters in tilted elliptical media; (b) estimation of stereotomography parameters in anelliptical media using only reflection and diffraction events and surface acquisition geometry is possible but can be ill-conditioned; (c) the inclusion of transmission events from VSP experiments improves the conditioning of stereotomography; (d) the determination of the orientation of the slowness curve together with the position of the diffraction or reflection point is ill-conditioned. On this basis, we have provided a possible formulation for the necessary regularization for the anisotropic problem.

Numerical examples demonstrated that isotropic stereotomography in anisotropic media tends to produce systematic localization errors. The use of anisotropic stereotomography improves the focusing and localization of diffractors, but only if additional transmission data are taken into account. Therefore, a macrovelocity model that is useful for migration can only be constructed by stereotomography if both types of events are available.

ACKNOWLEDGMENTS

We thank the Consortium "Seismic waves in complex 3D structures (SW3D)" and Ivan Pšenčík for the ray tracer ANRAY. We thank the Brazilian Agencies ANP, CNPq, FAPESP, and FINEP, as well as PETROBRAS and the sponsors of the Wave Inversion Technology (WIT) Consortium for financial support.

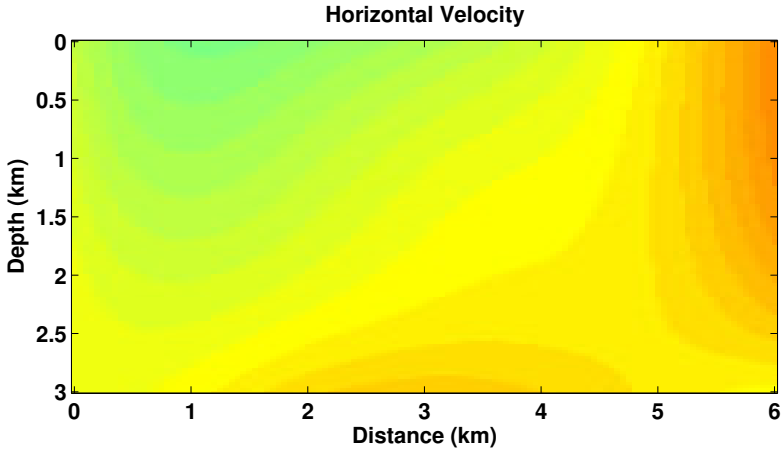

Figure 18: Horizontal velocity as result of elliptic stereotomography.

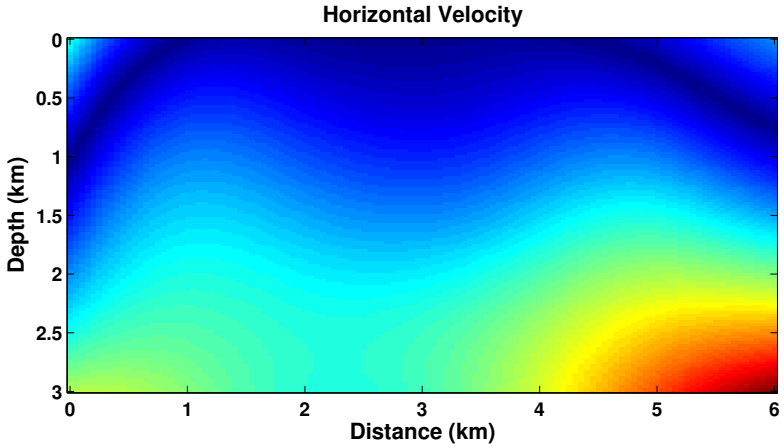

Figure 19: Relative error of horizontal velocity from elliptic stereotomography.

REFERENCES

Billette, F. and Lambaré, G. (1998). Velocity macro-model estimation from seismic reflection data by stereotomography. *Geophys. J. Int.*, 135(2):671–690.

Billette, F., Le Bégat, S., Podvin, P., and Lambaré, G. (2003). Pratical aspects and applications of 2D stereotomography. *Geophysics*, 68(3):1008–1021.

Bishop, T. N., Bube, K. P., Cutler, R. T., Langan, R. T., Love, P. L., Resnick, J. R., Shuey, R. T., Spindler, D. A., and Wyld, H. W. (1985). Tomographic determination of velocity and depth in laterally varying media. *Geophysics*, 50:903–923.

Červený, V. (2001). *Seismic Ray Theory*. Cambridge University Press.

Dellinger, J., Muir, F., and Karrenbach, M. (1993). Anelliptic approximations for TI media. *J. Seis. Expl.*, 2:23–40.

Farra, V. and Madariaga, R. (1987). Seismic waveform modeling in heterogeneous media by ray perturbation theory. *J. Geophys. Res.*, 92:2697–2712.

Farra, V. and Madariaga, R. (1988). Non-linear reflection tomography. *Geophysical Journal*, 95:135–147.

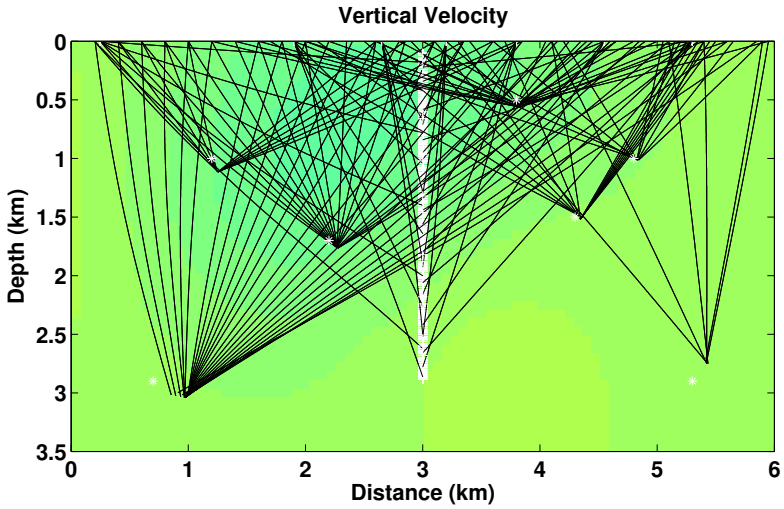

Figure 20: Vertical velocity as result of anelliptic stereotomography.

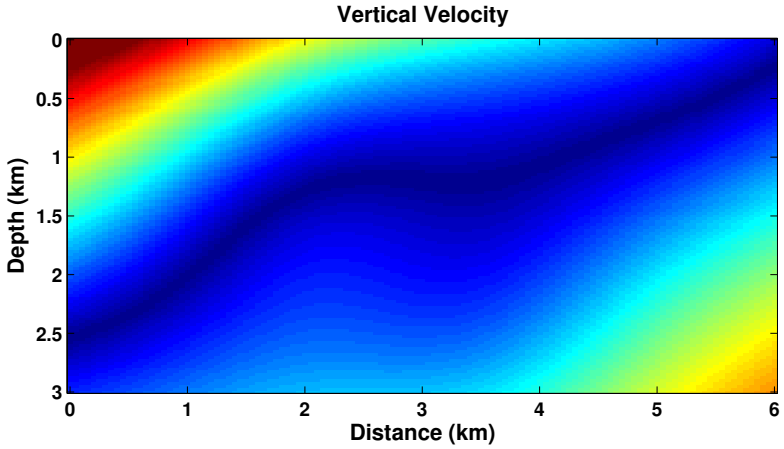

Figure 21: Relative error of vertical velocity from anelliptic stereotomography.

Gajewski, D. and Pšenčík, I. (1990). Vertical seismic profile synthetics by dynamic ray tracing in laterally varying layered anisotropic structures. *J. Geophys. Res.*, 67(1):300–306.

Goldstein, H. (1980). *Classical Mechanics*. Addison Wesley series in physics, 2nd edition.

Gosselet, A., Le Bégat, S., and Petersen, S. (2005). Joint slope tomography of borehole transmitted and surface seismic data. In *75th Annual International Meeting, SEG, Expanded Abstracts*, pages 2577–2580.

Lawson, C. L. and Hanson, R. J. (1974). *Solving Least Squares Problems*. Prentice-Hall, Inc.

Menke, W. (1989). *Geophysical Data Analysis: Discrete Inverse Theory*, volume 45 of *International Geophysics*. Academic Press, 2nd edition.

Musgrave, M. J. P. (1970). *Crystal Acoustics*. Holden-day.

Nolet, G., editor (1987). *Seismic Tomography*. Reidel, Dordrecht, the Netherlands.

Schoenberg, M. and deHoop, M. V. (2000). Approximate dispersion relations for qP-qSV-waves in transversely isotropic media. *Geophysics*, 65(3):919–933.

Thomsen, L. (1986). Weak elastic anisotropy. *Geophysics*, 51(10):1954–1966.

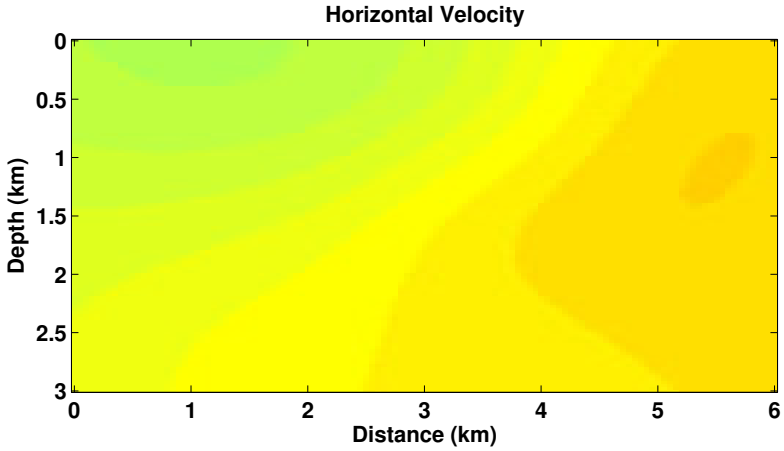

Figure 22: Horizontal velocity as result of anelliptic stereotomography.

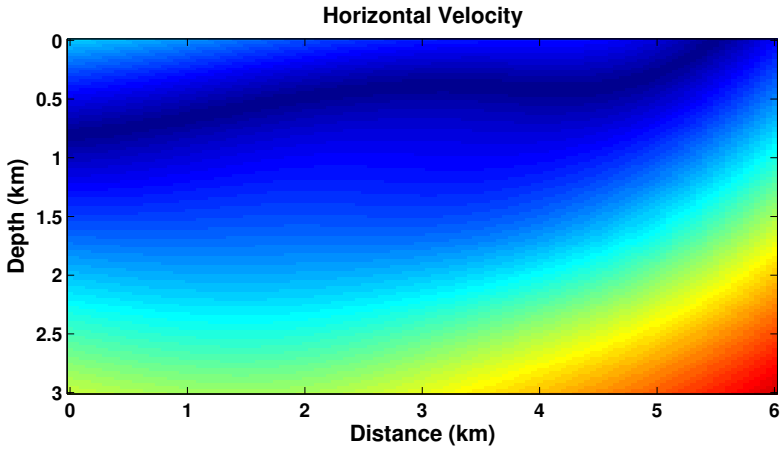

Figure 23: Relative error of horizontal velocity from anelliptic stereotomography.